Gasification and physical-chemical characteristics of carbonaceous materials in relation to HIsarna ironmaking process

Theint Theint Htet[1], Zhiming Yan[1*], Stephen Spooner[1], Volkan Degirmenci[2], Koen Meijer[3], Zushu Li[1]

1. WMG, University of Warwick, Coventry, CV4 7AL, UK
2. School of Engineering, University of Warwick, Coventry, CV4 7AL, UK
3. IJmuiden Technology Centre, PO Box 10000, 1970 CA IJmuiden, The Netherlands.
* Corresponding Author:
Zhiming Yan, E-mail: Zhiming.Yan@warwick.ac.uk

Abstract

HIsarna ironmaking process is one of the emerging technologies being developed to mitigate the increasing carbon footprint from the steel making industry. This innovative process offers flexibility with the type of reductants used in the smelting reduction vessel for the conversion of iron ore to liquid hot metal. Natural gas is well known for being a relatively clean fossil fuel producing carbon black and hydrogen when it undergoes thermal decomposition. The gasification reactivity of carbon black compared to the carbonaceous materials used in HIsarna process is investigated in this work using isothermal gravimetric analysis (TGA) method at 1250˚C, 1350˚C and 1450˚C under atmospheric pressure. Furthermore, physical-chemical characteristics of the individual carbonaceous materials, which may influence the reactivity, are evaluated systematically. The experimental results show that carbon black is the least reactive followed by thermal coal and charcoal. It was found that the effect of the morphology of the carbonaceous materials on the reactivity is dominant compared to the surface area of the materials. In addition, the reactivity increases with the alkali index (AI) and the level of the amorphousness of the material's structure. Three well-known kinetic models, i.e. the volumetric model (VM), the grain model (GM) and the random pore model (RPM) were applied to predict the gasification behaviour of the three carbonaceous materials. The random pore model best describes the gasification reaction of the selected samples due to the influence of the pore diffusion on the reaction. It is observed that the activation energy of the samples are not following the order of reactivity, this can be explained by the kinetic compensation effect.

Keywords: smelting reduction; CO_2 gasification; charcoal; thermal coal; carbon black; reactivity

1. Introduction

The steel industry is ranked as one of the highest CO_2 emitters due to the use of coal as a primary reductant for iron and steel production[1]. It is currently responsible for 6% of the total world anthropogenic CO_2 emission and in the EU, CO_2 emission is 1.8 tonnes per tonne of crude steel produced through the blast furnace-basic oxygen furnace (BF-BOF) route[2]. The global demand for steel which has a potential to increase up to approx. 2200 (Million tonnes) Mt by 2050[1] may result in enormous increase in carbon footprint. In order to mitigate the increasing CO_2 emission from the steel industry, the research and development initiatives around the world have been investigating alternative ironmaking processes under CO_2 breakthrough programmes[3]. In Europe, the ULCOS (Ultra Low CO_2 steelmaking) programme, involving major European steel companies, suppliers and associations was established in 2004 to reduce CO_2 emission by at least 50% by 2050 compared to 1990 level[4,5]. HIsarna is one of the emerging ironmaking technologies developed by Tata Steel as part of the ULCOS. The process involves the two main technologies, cyclone and HIsmelt technology, **Figure 1**. The cyclone melts the ore, fluxes, and pre-reduces the ore, whilst HIsmelt technology provides the final reduction of the liquid pre-reduced ore and coal gasification in the smelting reduction vessel (SRV). It aims to reduce the CO_2 emissions up to 80% by 2050 with the combination of carbon capture and storage (CCS)[6,7]. One of the main advantages of this process is the flexibility to use alternative reductants to the current standard metallurgical coal. The CO_2 reduction efficiency of HIsarna's pilot plant has previously been demonstrated using thermal coal (TC) and charcoal (CC) as the alternative reductants. Further information on HIsarna and its current progress/development can be found in the reported literature[6-10]. A potential alternative of interest is to utilise natural gas in smelting reduction vessel (SRV) as a partial replacement of coal and biomass[11]. If natural gas is used as a carrier gas for the injection of coal into the slag/hot metal interface, upon rapid heating, it may crack into carbon and hydrogen. The cracked carbon may react with the HIsarna slag and carburise the hot metal. Previously, natural gas has been used as a co-reductant in the ratio of 125 kg/t hot metal, with the gas containing primarily methane in the North America's blast furnaces as a partial replacement of coke[12]. Natural gas is also extensively used in direct reduction processes, like MIDREX that accounts for 60% global direct-reduced iron (DRI) production[19]. This previous work provides precedent to the potential successful application of natural gas in HIsarna.

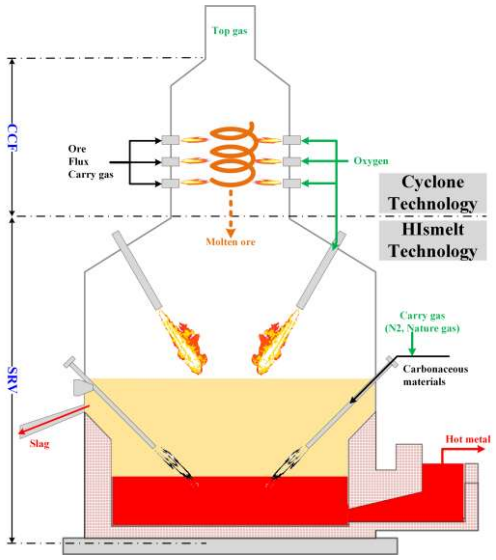

Figure 1 Schematic diagram of the HIsasrna furnace involving two integrated technologies[7]

Natural gas is well known for being a relatively clean fossil fuel due to generation exclusively of elemental carbon and hydrogen through thermal decomposition (equation (1)), which are two common reductants for the reduction of iron oxide for the iron production[11,12]. Consequently, it may aid lowering the carbon in the process and ultimately the CO_2 emissions.

$$CH_4 \xrightarrow{\Delta} C + 2H_2 \quad (1)$$

The elemental carbon produced is known to be carbon black (CB) containing more than 97% carbon[14], which contrasts with TC and CC containing approximately 81.9% and 89.4% carbon respectively. Moreover, cracked CB is a nano-material, known as active carbon which is applicable in making consumer products such as rubber, inks, paints and coating[14,15]. No information has been reported on the reaction between the cracked CB and solid carbon materials with iron oxides under HIsarna conditions. Therefore, the reduction behaviour of CB, and the solid reductants used in HIsarna with slag containing iron oxide is an area that needs further study in order to aid the potential application.

Within the SRV, moisture and other volatile matters from solid carbon sources are reportedly released immediately into the molten slag upon injection due to the high temperature within the vessel[6,7,16].

Then, the reduction of iron oxide may occur via two main reactions: (1) direct reduction, and (2) indirect reduction[17-20]. The direct reduction occurs initially through the direct contact between the devolatised carbon and iron oxide in slag, producing CO (equation (2))[18-27]. The product gas, CO forms a gas film between molten slag and the carbon[18-27]. The iron oxide in the molten slag can then be further reduced by the product gas, and as a result, CO_2 is generated (equation (3))[18-27]. This gaseous reaction is known as indirect reduction. During the

indirect reduction, a gas ferrying mechanism may occur[21,22]. This is due to the CO_2 traveling from the slag/gas interface to gas/carbon interface, producing more CO through gasification reaction or Boudouard reaction (equation (4)), which travels in the reverse direction of the CO_2[21,22]. This mechanism is shown schematically in **Figure 2**. Previous studies[18,19,28] stated that the mass transfer of iron oxide from bulk slag phase to the slag/gas interface is the controlling step for the reduction rate when FeO % in the slag is less than 5%. However, the gasification reaction plays a significant role due to the contribution of the indirect reduction. Furthermore, the rate of the gasification reaction is dependent on the types of carbon in terms of their physical and chemical properties, consequently it may likely have impact on the overall reduction rate of iron oxide.

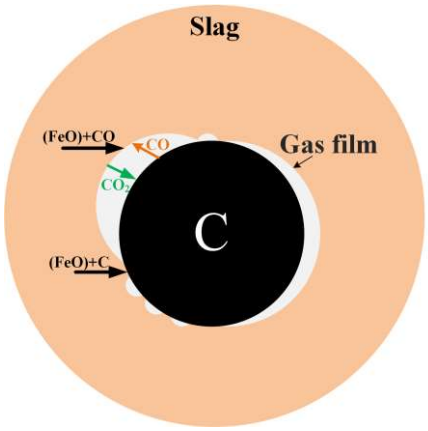

$$(FeO) + C\,(s) = [Fe] + CO\,(g) \quad (2)$$

$$(FeO) + CO\,(g) = [Fe] + CO_2\,(g) \quad (3)$$

$$CO_2\,(g) + C\,(s) = 2\,CO\,(g) \quad (4)$$

Figure 2 Illustrative diagram of the reaction mechanism between the molten slag and a carbon particle.

The CO_2 gasification behaviour of various solid carbon materials such as coal and biomass char has been widely reported in the past for both non-isothermal and isothermal studies[29-32]. The majority of the research has focused on the gasification reactivity of the individual carbon materials, which may significantly influence the overall operating efficiency and economic benefits of syngas production plants or gasification plants[30-33]. Hence, the reported studies[30-33] were mostly conducted around the industrial gasification plant's operating conditions, around 1000˚C and below. The CO_2 gasification behaviour of CB, TC, and CC under HIsarna operating conditions at 1450˚C, is an area that needs research.

The present work aims to investigate the gasification properties and kinetic behaviours of CB and the carbonaceous materials (TC and CC) previously used in HIsarna trial campaigns using isothermal thermogravimetric analysis (TGA) at high temperature range of 1250-1450˚C. The major factors which may influence the reactivity of the gasification reaction such as morphology (e.g. particle shape and porosity), chemical structure, surface area, chemical composition of the materials are evaluated, which is coupled with

kinetic analysis of the reaction through the well-known kinetic models i.e., Volumetric model (VM), Grain model (GM), and Random pore model (RPM).

2. Experimental

2.1. Materials preparation

Three types of carbon materials, i.e. CB, TC and CC, were investigated in the present work. The lumps of TC and CC were provided by Tata Steel. The samples were heated at 70 °C in a muffle furnace for 12 hours in order to remove the surface moisture. The dried samples were crushed using a TEMMA disc mill with stainless steel mill plates and subsequently sieved to obtain samples with a particles size of between 63-90 µm for the test. The proximate and ultimate analysis results of the materials are given in **Table 1.**

Table 1 Proximate and ultimate analyses (dry basis) of charcoal and thermal coal provided by Tata Steel Europe, IJmuiden

Sample	Proximate analysis (wt.%)			Ultimate analysis (wt.%)				
	Volatile	Fixed carbon	Ash	H	O	N	S	C
CC	12.1	81.5	1.8	3.1	6.9	0.57	0.1	89.4
TC	22.2	60.1	8.8	4.3	11.4	2.2	0.2	81.9

CB was produced through the thermal decomposition of methane gas using a bespoke lab gas furnace, **Figure 3(a)**. The gas furnace is designed to operate at atmospheric pressure and under a controlled atmosphere. This water-cooled furnace is equipped with the graphite heating element and can be heated up to 1600˚C. Initially, the furnace was heated under argon (N5.0, 99.999%) until the temperature reached at 1450˚C. Once it reached the temperature, ultra-high purity (N 5.5, 99.9995%) methane gas was introduced into the furnace through the top injection lance (a schematic of which is shown in **Figure 3(b)**), generating solid carbon black which contains > 97% elemental carbon and hydrogen. The generated hydrogen was transported to the gas burner via top and side exhaust lines, where the reactive gas was burned. The by-products gases from the burner were discharged into the atmosphere via the extractor. The solid particles are collected at room temperature and the composition of the carbon black is shown in **Table 2**.

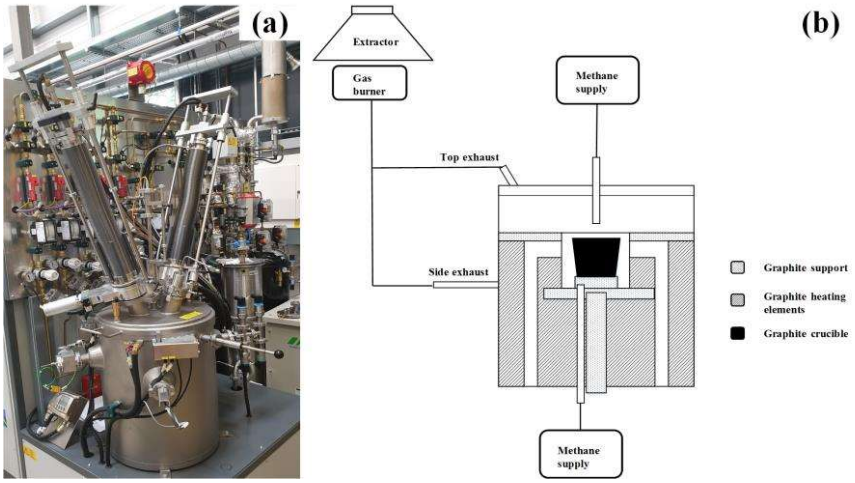

126

127 **Figure 3 Picture of the bespoke lab gas furnace (a) and a schematic diagram of the bespoke lab gas furnace (b)**

128 **Table 2 Composition of the carbon black[14].**

Sample	Elemental carbon	Ash content	Organic
Carbon black	>97%	<1%	<1%

129

130 The morphology of the raw materials before and after heating were observed by using a Sigma Zeiss SEM
131 (scanning electron microscopy) under the imaging conditions of 5kV voltage, 1,000 times magnification for TC
132 and CC, and 10,000 and 26,000 times for CB as they are nano-particles. The Brunauer-Emmett-Teller (BET)
133 surface areas and porosity of the samples (raw and char) were determined by nitrogen adsorption method at
134 77K. The samples were heated under vacuum at 120˚C for 12 hours with the purpose of degassing the samples.
135 The degassing step was repeated two times prior to the BET test. Moreover, the structure of the chars were
136 studied by Raman spectroscopy method. Raman spectra for the sample chars produced at 1450˚C are obtained
137 using a Renishaw spectrometer equipped with a silicon-based Charge Coupled Device (CCD) detector. The
138 measurements were made in the range of between the wavenumber of 1000 cm^{-1} and 1800 cm^{-1} under a green
139 laser (wavelength, λ= 532nm). The laser power of 5% and 20s exposure time are chosen in order to avoid
140 irreversible thermal damage to the samples. The spectra from three different locations from each sample were
141 recorded due to the heterogeneous nature of the samples. The recorded spectra are analysed using the peak
142 analysis function in *OriginPro 2019b*.

143 **2.2. Gasification test**

144 One of the most commonly used methods to investigate the gasification of the carbonaceous materials is thermal
145 gravimetric analysis (TGA)[29-32]. In this study, a NETZSCH STA 449 F3 Jupiter was used for the TGA analysis.
146 At the start of each experiment, approximately 15 mg of the sample was placed in an alumina crucible (4 mm in

147 height and 6.8 mm ϕ). A small amount of sample was used to avoid heat transfer limitation, which was essential
148 to ensure that the results had a good reproducibility. The crucible containing the sample was then covered with
149 an alumina lid with a central hole. The temperatures for isothermal experiments were selected to be 1250˚C,
150 1350˚C, and 1450˚C. The sample was heated at a rate of 30˚C min^{-1} under Argon (N5.0, 99.999%) until it
151 reached the target temperature. The sample was then held at the target temperature for 10 minutes under inert
152 atmosphere in order to have a stable weight before CO_2 was then introduced for gasification. The argon was
153 replaced by carbon dioxide (N5.0, 99.999%) with the flowrate of 50 ml/min in order to have the minimal
154 resistance around the particles resulting from the stagnant gaseous film[29]. The final temperature was kept for
155 gasification until no further weight loss could be observed. Each test was repeated at least three times to ensure
156 experimental rigor. Furthermore, a blank calibration test was run for each temperature with the crucible
157 containing 15 mg of alumina powder.

158 **2.3 Kinetic Models**

159 The experimental conversion (X_{exp}) of the three kinds of carbon used in this study (on a dry ash-free basis) via
160 the gasification process can be determined using equation (5):

161 $$X_{exp} = \frac{m_i - m_t}{m_i - m_{ash}} \quad (5)$$

162 Where, m_i denotes the initial sample mass before the gasification; m_t is the sample mass at time t; m_{ash} is the
163 mass of remaining ash in the sample after the reaction is complete.

164 The gasification of carbon can be considered as non-catalytic heterogeneous reaction. Hence, the conversion
165 rate of the CO_2 gasification of carbon *dX/dt* can be expressed by equation (6)[31]:

166 $$\frac{dX}{dt} = k\left(T, P_{CO_2}\right) f\left(X\right) \quad (6)$$

167 where, *k* is the apparent gasification rate constant influenced by temperature *(T)* and CO_2 pressure P_{CO2}. *f(x)*
168 gives the dependency of physical and chemical properties with the relation to degree of reaction.

169 In the case of constant CO_2 pressure during the reaction, the apparent gasification reaction rate constant can be
170 determined by the Arrhenius equation, equation (7):

171 $$k = A_0 e^{\left(-\frac{E}{RT}\right)} \quad (7)$$

172 Where, A_0, *E* and *R* represent pre-exponential factor, activation energy and universal gas constant respectively.

173 Linearized Arrhenius equation is shown in equation (8):

$$\ln k = \ln(A_0) - \frac{E}{R}\left(\frac{1}{T}\right) \quad (8)$$

In this study, three well-known kinetic models were adopted to predict the gasification rate of the three carbonaceous materials under different conditions. The description of these three models can be found in **Table 3**. The linearized equations of the individual models were used to obtain the predicted conversion value (X) of the samples.

Table 3 Three kinetic models for the prediction of the gasification of the three carbonaceous materials.

Models	Governing equations	Remarks
Volumetric model (VM)[31]	• $\frac{dX}{dt} = k_{VM}(1-X)$ (9) • $-\ln(1-X) = k_{VM}t$ (10) • $X = 1 - e^{(-k_{VM}t)}$ (11) Where, k_{VM} denotes apparent gasification rate constant of VM model.	The model does not consider the structural changes of the particles during the reaction, assuming that there are uniformly distributed active sites on both the outside and inside the particle surface, which are reacting with the oxidising agents.
Grain model or unreacted core model (GM) [32]	• $\frac{dX}{dt} = k_{GM}(1-X)^{2/3}$ (12) • $3\left[1-\left(1-X\right)^{(1/3)}\right] = k_{GM}t$ (13) • $X = 1-(1-k_{GM}t/3)^3$ (14) Where, k_{GM} denotes apparent gasification rate constant of GM model.	The model assumes that a porous particle contains an assembly of uniform nonporous spherical grains. The reaction occurs on the external surfaces of the grains and gradually moves inside. During the reaction, unreacted core behaviour is applied to each of these grains. As the reaction continues, only the ash layer remains.
Random pore model (RPM)[40]	• $\frac{dX}{dt} = k_{RPM}(1-X)\sqrt{1-\psi\ln(1-X)}$ (15) • $\left(\frac{2}{\psi}\right)\left[\left(1-\psi\ln\left(1-X\right)\right)^{\frac{1}{2}}-1\right] = k_{RPM}t$ (16) • $X = 1-e^{\left(-k_{RPM}t\left(1+\frac{k_{RPM}\psi}{4}\right)\right)}$ (17) Where, k_{RPM} is apparent gasification rate constant of RPM model, ψ pore structure of the non-reacted sample.	The model considers the pore structure and its evolution; pore growth during initial stages of gasification and destruction of pores due to the coalescence of adjacent pores.

The kinetic models used in this study can be validated through the comparison between the experimental and predicted conversion values. The deviation (DEV) between the experimental data and predicted data can be determined by equation (18)[31].

$$DEV(X)(\%) = 100 \times \left(\sum_{j=1}^{N} \frac{\left(X_{\exp,j} - X_j\right)^2}{N} \right)^{\frac{1}{2}} / max(X)_{exp} \quad (18)$$

Where, $DEV(X)(\%)$ is relative error: $X_{exp,j}$ is experimental data; X_j is the predicted data by the models; $max(X)_{exp}$ is the maximum conversion of the experiment; N is the number of data points.

3. Results & Discussion

3.1. Iso-thermal gravimetric analysis

In order to predict the kinetic behaviour of the studied materials, and to validate the selected kinetic models, the experimental data was fitted to the different kinetic models using a least square non-linear curve fitting method. The plots of conversion against time for both experimental and model fitted graphs are presented in **Figure 4 (a) – (i)**. The duration of 2000s is considered for the conversion of all the studied carbon types. The rate constants for all the chosen models, k_{VM}, k_{GM} and k_{RPM}, and the value of ψ in the RPM model are determined from the slope of the optimum curve fitting. The latter value is constant and independent of the temperature as it represents the original pore structure of the particles[31]. The values of ψ for the studied samples vary between 17 and 20. The Arrhenius plot, **Figure 5** is attained by plotting the natural logarithm of the calculated rate constants against inverse temperature. The gasification of the carbonaceous materials may occur under one kinetic control regime as there is a good linear relation between the *lnk* and *1/T* under varied temperatures[31]. The activation energy *(E)* and pre-exponential factor (A_0) in **Table 4** are obtained from the slope and interception of the plot respectively. The activation energy *E* of the selected samples vary between 42.5 – 89.0 kJ/mol, and A_0 is 2.9-149.2 s^{-1}. The ranking of the activation energy for the studied samples is: TC char > CC char > CB. The activation energy values obtained in this study are significantly lower than the literature values in Table 5, which were studied at temperature 1050 ˚C and below. This can be explained as the reaction may occur under mixed control regime rather than just the chemically-controled regime at high temperature range, where the influence of pore diffusion becomes significant [38,39].

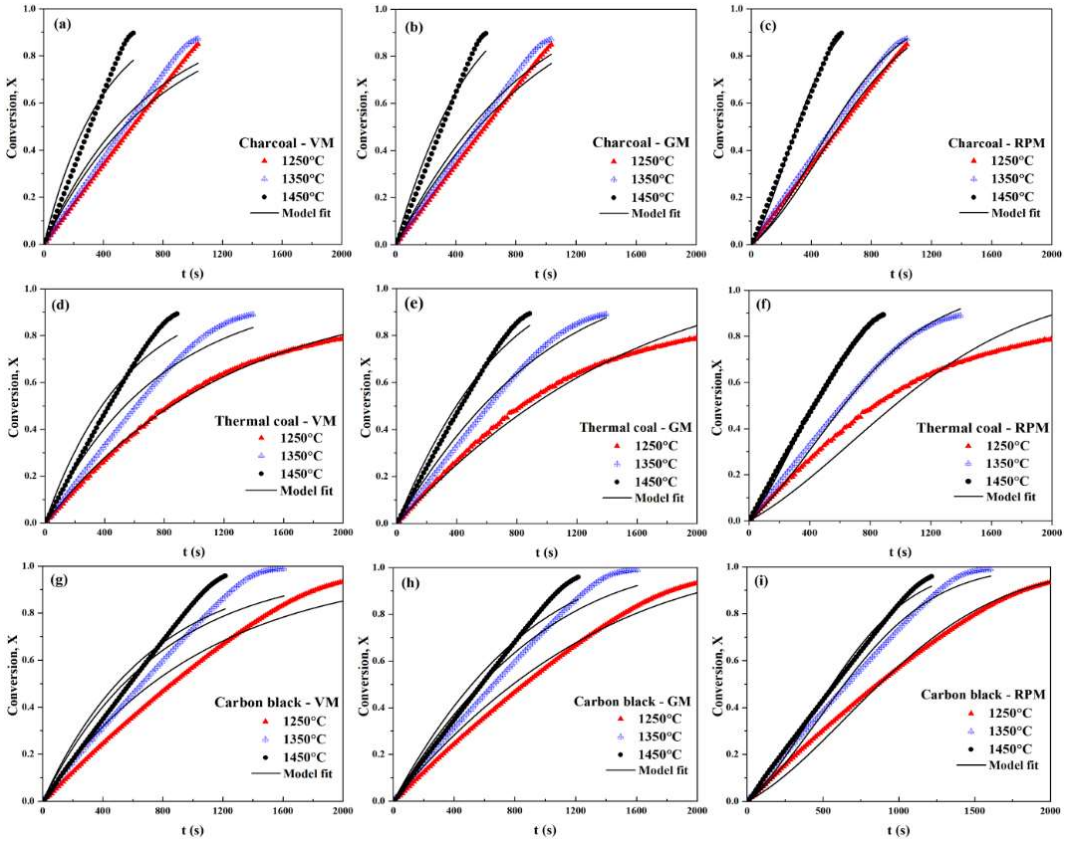

Figure 4 Non-linear curve fitting of experimental data using VM, GM and RPM models for (a) CC-VM, (b) CC-GM, (c) CC-RPM, (d) TC-VM, (e) TC-GM, (f) TC-RPM, (g) CB-VM, (h) CB-GM, and (i) CB-RPM.

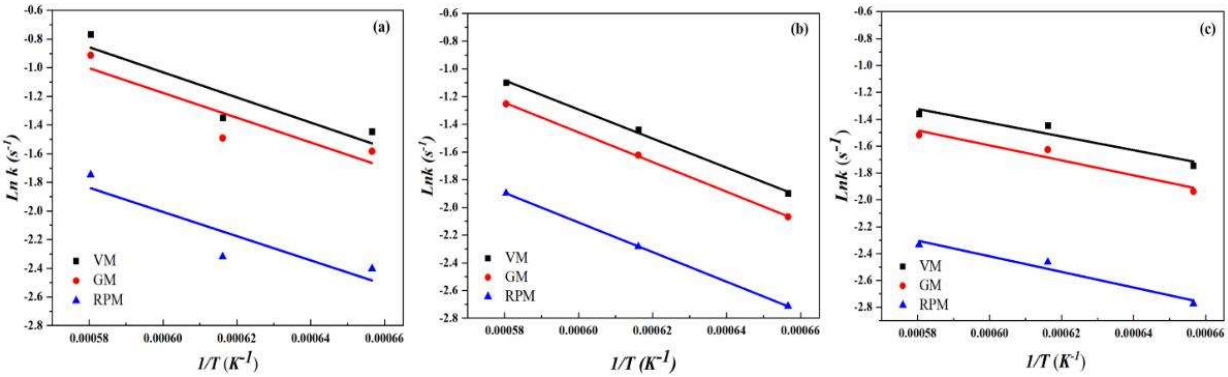

Figure 5 Arrhenius plots of VM, GM and RPM models for (a) Charcoal, (b) Thermal coal, and (c) Carbon black.

According to **Figure 4**, the RPM model has the best fitting for the gasification reaction of the studied materials as opposed to VM and GM models since the RPM model considers the pore structure of the materials. This result agrees well with the literature[31,32,35,38-40]. However, in the case of TC at 1250˚C, the VM model produces the best fit line for the experimental data of the reaction, whereas the RPM model deviates significantly from the experimental data. The deviation percentage between the predicted data and the experimental data for all set of experiments are calculated using equation (18) and the calculated results are displayed in **Table 6**. The calculated deviation percentage of the RPM for TC at 1250˚C is 5.3%, while the VM model is 0.9%. This could

be due to the non-porous nature of thermal coal and the pore evolution of TC char at 1250˚C not being dominant. As the sample was heated to the higher temperature, RPM model predicts better for TC compared to the other two models due to the coal swelling and large pore evolution of TC char[35]. This is further explained qualitatively by the SEM images of before and after heating the samples to specific temperatures as shown in **Figure 6 (a)-(h)**.

Table 4 Kinetic Parameters for VM, GM, RPM of different samples obtained from Arrhenius plots & models fitting to experimental data

Sample	VM		GM		RPM		
	E (kJ/mol)	A_0 (s^{-1})	E (kJ/mol)	A_0(s^{-1})	E (kJ/mol)	A_0 (s^{-1})	ψ
CC	81.2	68.7	71.9	55.2	70.3	21.4	20
TC	87.3	149.2	89	143.7	88.9	74.3	12
CB	42.5	5.2	46.3	5.7	48.3	2.9	18

Table 5 Activation energy values of coal and biomass chars reported in the literature for gasification reaction

	Model	E (kJ/mol)	Materials	Temperature (˚C)	Particle size (µm)
Wang et al.[31]	RPM	129.8-180.3	Herbaceous & wooden residues	800-950	< 74
Seo et al.[36]	RPM	134	Biomass char (*Pinus densiflora*)	850-1050	250-300
Li and Cheng[37]	-	122	Wu Tai gas coal	850-960	2000-4000
Sircar et al.[38]	RPM	125.0± 30	Pinewood char	727-897	56-180

Table 6 Deviation between the predicted data by the models and the experimental data

Sample	*DEV X* (%) 1250˚C			*DEV X* (%) 1350˚C			*DEV X* (%) 1450˚C		
	VM	GM	RPM	VM	GM	RPM	VM	GM	RPM
CC	6.5	4.6	2.3	6.9	4.7	2.1	7.4	5.2	1.9
TC	0.9	2.5	5.3	4.9	2.7	1.2	6.3	4	1.6
CB	3.9	2.2	1	6.7	4.5	2.2	7.5	5.3	2.2

3.2. Morphology of the materials

The morphological changes of the samples before and after heating to the reaction temperatures of 1250˚C and 1450˚C are studied using SEM and the images are presented in **Figure 6.** The raw CC used in this study is very porous as shown in **Figure 6(a)**. It was observed that as pyrolysis temperature increases, more pores collapse causing the shrinkage of the material as shown in **Figure 6(b)**, and new pores form on the surface of the CC char particles after the shrinkage as shown in **Figure 6(c)**. The behaviour of the CC during the pyrolysis fits

well with the RPM model's considerations on pore structure and its evolution, therefore, the RPM model gives the best-fit line for the CC char (**Figure 4(c)**).

On the other hand, raw TC is non-porous according to the **Figure 6(d)**. After heating to 1250 ˚C, some tiny pores are evolved with some ash on the surface due to the release of volatile gas compounds (**Figure 6(e)**). Large pores are seen to evolve and the surface becomes cleaner after heating the TC to 1450 ˚C, from the release of more volatile matters, causing ruptures in the materials (**Figure 6(f)**). The pore evolution of TC at 1250 ˚C may not be dominant, hence the RPM model does not predict the experimental data well at that temperature (**Figure 4(f)**). However, at 1450˚C, the pore evolution of TC char becomes dominant, resulting in the RPM model giving the best fit (**Figure 4(f)**).

The morphology of CB does not change significantly after heating as shown in **Figure 6(g) and 6(h)** due to the material being produced at high temperature of 1450˚C. According to **Figure 6(g)**, carbon black has nano-particle size and a grape like cluster shape which follows the descriptions of previous studies[16]. Due to being nano-size particles, no pores are observed within individual particles of CB. However, aggregates are formed from the primary particles coming into contact, **Figure 6(g)**. Clustering of these aggregates may lead to form agglomerates, and the pore formation occurs between aggregates as in **Figure 6(h)**. The particles agglomeration and the pore formation are schematically presented in **Figure 6(i)**. Hence, the gasification of carbon black can be well represented by the RPM model (**Figure 4(i)**).

The reactivity of the samples at different temperatures are evaluated quantitatively according to their reactivity index, $R_{0.5}$ using equation (19)[31,40].

$$R_{0.5} = \frac{0.5}{t_{0.5}} \tag{19}$$

where, $t_{0.5}$ is the time required for half the sample to be converted.

The calculated reactivity index values are shown in Table 7. The higher the value of $R_{0.5}$, the higher the reactivity of the sample[31,32,40]. Therefore, CC is the most reactive material followed by TC and finally CB. Furthermore, the reactivity of all three materials studied increases with increasing the reaction temperature from 1250 ˚C to 1450 ˚C.

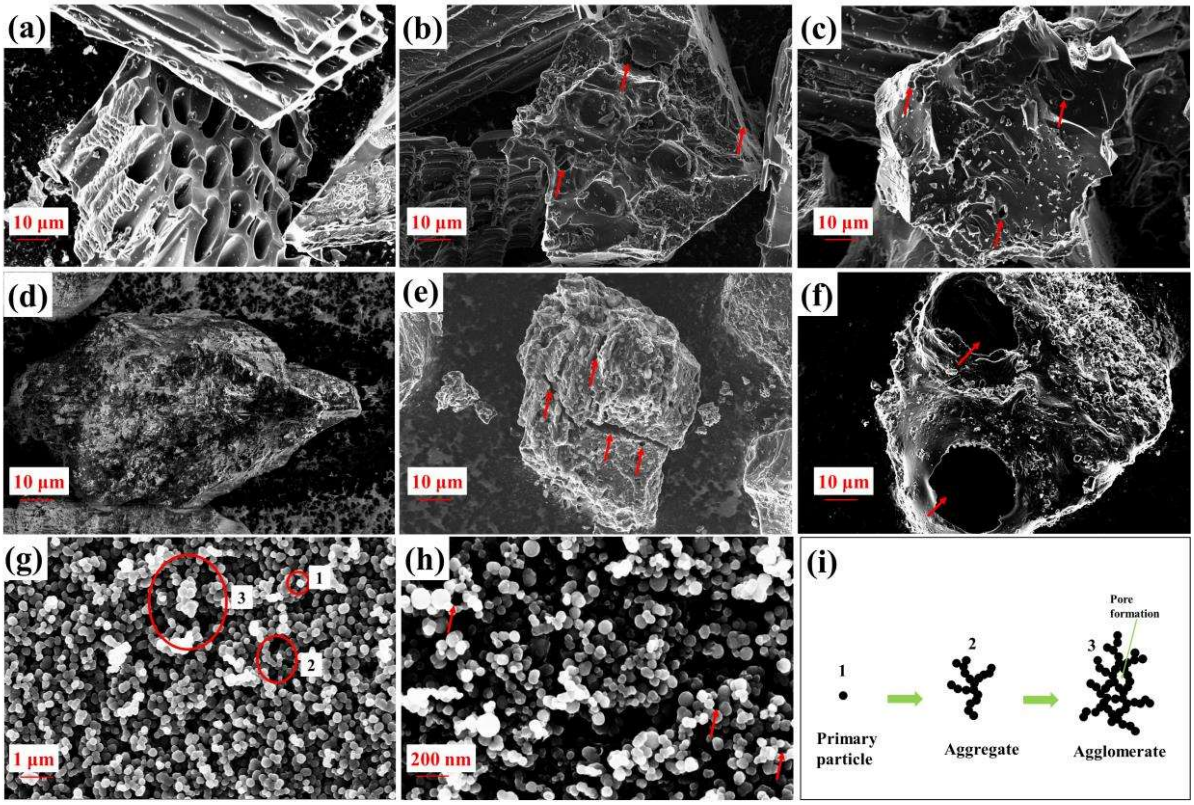

Figure 6 Comparison of SEM photographs of the three different samples before and after pyrolysis at various temperature: (a) CC raw, (b) CC char 1250˚C, (c) CC char 1450˚C, (d) TC raw, (e) TC char 1250˚C, (f) TC char 1450˚C, (g)CB raw, (h) CB 1450˚C, and (i) schematic view of CB agglomeration. All the SEM photos are taken under magnification of 1,000 except 10,000 for (g) and 26,000 for (h).

Table 7 Reactivity index of the studied samples at different temperatures.

	Temperature (˚C)	Charcoal char	Thermal coal char	Carbon black
Reactivity Index, $R_{0.5}$ x 10^{-4}	1250	8.3	6.0	5.8
	1350	9.0	8.1	7.6
	1450	15.9	11.5	8.6

Furthermore, surface area and porosity of the materials are investigated quantitatively, using N_2 adsorption technique (BET test). The adsorption isotherms of the materials and their physical parameters are displayed in **Figure 7** and **Table 8**. According to International Union of Pure and Applied Chemistry (IUPAC) recommendations[41], the isotherm of CC raw in **Figure 7** (a) belongs to type I, which indicates that the sample is microporous. The isotherm is found to be non-reversible resulting from the existence of a constricted microporous structure[42]. Moreover, the N_2 molecules move very slowly at 77K, hence the adsorption in very narrow pores is kinetically limited[31]. On the other hand, the isotherms of CC 1450˚C, TC raw, TC 1450˚C and CB raw in **Figure 7** (b)-(e) are type II[41]. This indicates more micro/mesopores exist in the samples. Different

shapes of adsorption isotherms result from different distribution of pores existing in various samples[31]. The morphology of CB before and after the pyrolysis, **Figure 6** (g) and (h) is not changed, hence the adsorption test is not done on the CB 1450˚C.

The BET surface area and pore parameters of the samples are shown in **Table 8**. CB gives the highest surface area among the raw carbonaceous materials owing to being a nano-size material. Hence, it was initially expected to have the highest reactivity. However, spherical particles are known to be less reactive compared to the irregular particles[43]. On the contrary, the surface area of TC raw is very small because it is non-porous.

According to **Table 8**, the average pore diameter for TC raw is the largest and for CC raw the smallest. The measured pore diameter of the TC raw could result from the rough surface of the samples. Moreover, the pore diameters of the CC and TC chars are significantly decreased. This could be due to collapsing of the original pores and evolution of smaller pores in the case of CC char, **Figure 6** (c), whereas pore formation occurs in TC char, **Figure 6** (f) resulting in the higher BET surface areas than the raw materials. Consequently, faster reaction rate is achieved with increasing temperature. The results indicate that the morphology of the materials such as particle shape and porosity of the samples may have more significant effect on the reactivity compared to the surface area of the individual samples studied.

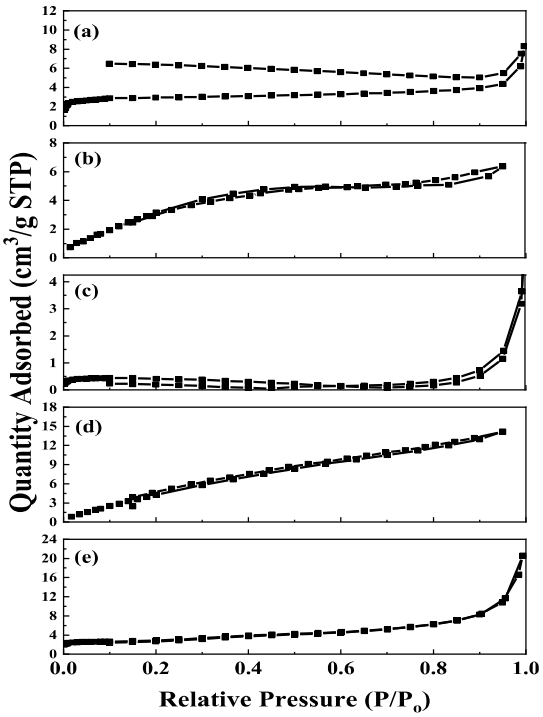

294

295 **Figure 7 BET nitrogen adsorption isotherms of raw materials and chars (a) CC raw, (b) CC 1450˚C, (c) TC raw, (d)**
296 **TC 1450˚C, and (e) CB raw.**

297 **Table 8 Parameters for physical properties of both raw carbonaceous materials and chars.**

Samples	BET surface area (m^2/g)	Cumulative pore volume (m^3/g)	Average pore diameter (nm)
CC raw	9.19	0.005738	13.94
CC char 1450˚C	14.31	0.005433	2.58
TC raw	1.14	0.004945	25.28
TC char 1450˚C	22.10	0.016686	3.37
CB raw	9.89	0.030688	14.31

298

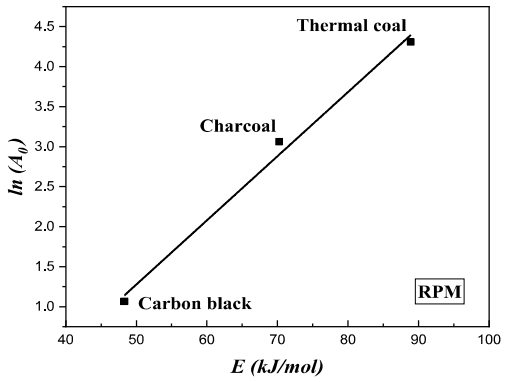

299
300 **Figure 8 The relation between *ln(A₀)* and *E* of different materials.**

It was found that the ranking of the activation energy of the samples do not follow the order of the reactivity index. In general, the lower the activation energy of the material is, the higher the reactivity is obtained, which is not the case in this study. According to Wang et al. 2016[31], this could be due to the reactivity being affected by not only activation energy but also by the pre-exponential factor. Under the circumstance of increasing pre-exponential factors with the increasing activation energies, kinetic compensation effect may occur[31]. **Figure 8** shows that there is an apparent linear relation between lnA_0 and E. The lower the activation energy, it is easier to attach CO_2 molecules to the active carbon sites to produce CO[46,47]. However, the stronger bond between C(O) is formed and the structure of the chars become more stable, which alternatively limits the movement of CO[31,41,42]. This could result in the lower pre-exponential factors[31,46,47].

3.3 Chemical structural effect on the gasification rate

Previous research reported that the chemical structure of the sample may take part in controlling the gasification rate[31,45,48]. Raman spectroscopy is the most common method to study the chemical structure of the materials. The focus of this study is to determine the reactivity of the carbonaceous materials at HIsarna's condition. Hence, the raman spectra are obtained for the samples that have been pyrolysed at HIsarna operating temperature of 1450˚C and they are presented in **Figure 9 (a)**.

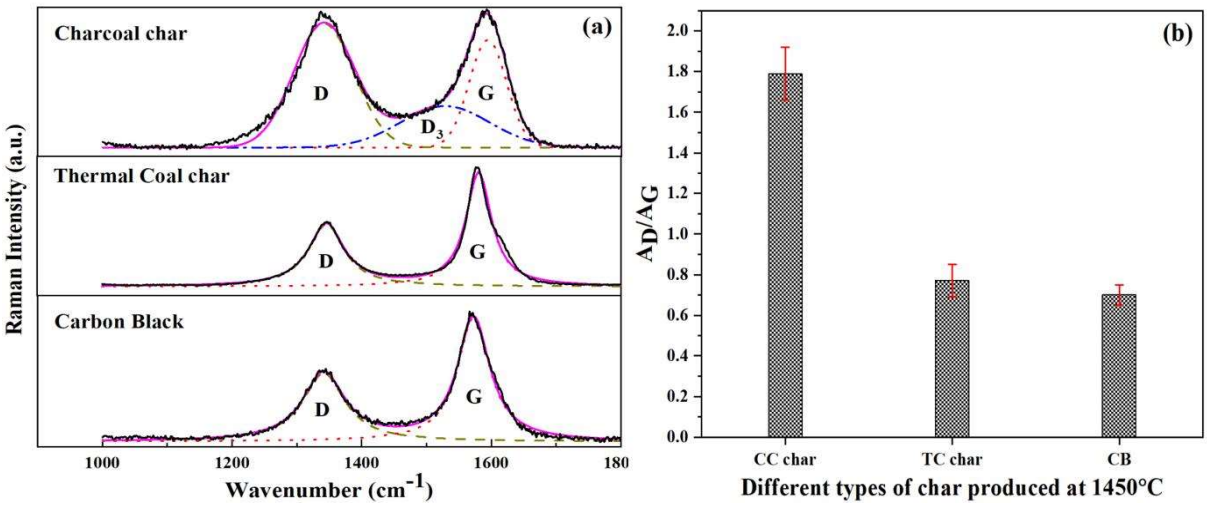

Figure 9 (a) Raman spectra of the carbonaceous materials with the respective peak fitting curves, and (b) Area ratio of D band and G band of the sample chars.

The two significant peaks occurred at ~1350 cm^{-1} and ~ 1600 cm^{-1} which are known as the D and G bands individually[48,33-51]. The disorder-induced D band corresponds to the contribution of amorphous carbon structure and G band is responsible for a stretching vibration mode of graphite C=C bonds[31,51]. The experimental spectra of CC char is deconvoluted into three peaks (D, D_3, and G) using Gaussian functions according to the method proposed by Sonibare et al., 2010[52]. The D_3 band occurs in the range of 1500 – 1550 cm^{-1} from the amorphous

Sp^2 bonded forms of carbon in the materials[51]. On the other hand, the spectra of TC char and CB are fitted with Lorentzian function[53]; only D and G bands are found.

From **Figure 9(a)**, the D and G bands of CC char are broader compared to the relevant bands of TC char and CB. The broader the G band of the material, the more amorphous structure of the material is obtained, hence CC char is more amorphous than TC char and CB[33,49]. The broad D band of CC char suggests that the crystallite size of the carbon in the materials is small, which further indicates that the material is highly amorphous[54]. On the contrary, the D and G bands of the TC char and CB are narrower and sharper, which proves that they are more highly ordered.

The ratio of the intensity of D and G bands, (I_D/I_G) are known to determine the degree of the organisation of the carbon materials; the intensity ratio increases with the increase in the degree of amorphousness[33-51]. The area ratios of D and G bands (A_D/A_G) are calculated in this study in order to obtain the most accurate result, and the results are displayed in **Figure 9(b)**. The area ratios of CC char, TC char, and CB are approx. 1.79, 0.78 and 0.67 respectively. Hence, the level of amorphousness is as follows: CC char > TC char > CB. Wang et al.,[31] claimed that the more disorder the structure is, the more chemically reactive under oxidation atmosphere. The result obtained in this study agrees well with the literature as the reactivity of the materials follows the trend of the amorphousness.

3.4 Effect of ash composition on the gasification rate

Generally the carbonaceous materials contain both volatile and ash matters which may influence the gasification reactivity. The role of volatile matter is not considered in this study, as the reaction happens at above de-volatilisation temperature, and the starting mass comparison is taken after 10 minutes at the reaction temperature for standardisation. Contradictory results are reported regarding the effect of ash contents on the reactivity depending on the type of samples and the experimental conditions. Some studies claimed that the ash content in coal and biomass does not have any effect on the reactivity[29,31,32], whereas other researchers reported that the minerals contained in the ash such as calcium, potassium, and sodium increase the reactivity[44,45,55-57]. Zhang et al, 2010[40] claimed that calcium enhanced the reactivity at the lower conversion of coal chars, < 0.4, while potassium encouraged the reactivity with increasing conversion. It has been reported that the inorganic elements such as potassium, calcium, magnesium, sodium, and iron have a catalytic nature, whereas silicon and aluminium are known to have inhibiting effect on the reaction[32,45]. Hence, the effect of ash content on the reactivity of the studied samples is investigated. This is done through comparison of the alkali index (AI)

[32,33,44,45] for TC and CC. The alkali index for CB is not calculated and assumed very low since it contains only <1 % ash.

$$AI = Ash \times \frac{Fe_2O_3 + CaO + MgO + Na_2O + K_2O}{SiO_2 + Al_2O_3} \quad (20)$$

The calculated *AI* values of the samples are ranked as follows: CC > TC > CB and the values are shown in **Table 9**. It shows a good relationship with the reactivity index. Hence, it may be concluded that the reactivity of individual materials are affected by their ash compositions.

Table 9 Ash composition and Alkali Index of the studied samples

Sample	Fe_2O_3	CaO	MgO	Na_2O	K_2O	SiO_2	Al_2O_3	AI
CC	2.94	14.80	1.63	1.90	5.31	61.50	7.65	4.38
TC	0.00	11.16	2.90	0.35	1.58	41.56	22.86	2.18

4. Conclusions

In order to optimise the use of reductants in HIsarna ironmaking process, the CO_2 gasification reactivity of three carbon materials of thermal coal, charcoal and carbon black (the decomposition product of natural gas) and the influencing factors have been studied. The following conclusions can be obtained:

- The carbon black produced from the thermal decomposition of natural gas is the least reactive followed by thermal coal and charcoal.
- The random pore model (RPM) gives the best prediction of the CO_2 gasification reaction for the samples studied, except the thermal coal char at 1250˚C due to the morphology of the sample. The activation energies of the studied samples obtained from the RPM model fall within 48.3-88.9 kJ/mol and kinetic compensation effect occurs during the gasification process.
- The effect of the morphology of the particles such as particle shape, pore structure and its evolution within the samples exceeds the influence of the surface area on the reactivity of the studied materials. Hence, the surface area of the individual materials may not have significant influence on the reactivity.
- Furthermore, the reactivity increases with increasing temperature, and with the degree of amorphousness of the materials. The degree of amorphousness of the three carbonaceous materials studied in the descending order is: charcoal char > thermal coal char > carbon black.
- The reactivity of the individual materials is also governed by their ash content (alkali index). The alkali index of the three carbonaceous materials in the descending order is: charcoal > thermal coal > carbon black.

Acknowledgement

Theint-Theint Htet highly appreciates Tata Steel Europe in IJmuiden for the full PhD studentship. Zushu Li would like to acknowledge the financial support from EPSRC under the grant number EP/N011368/1 (EPSRC Fellowship).

References

1. Hasanbeigi, A., Arens, M. and Price, L. (2014). Alternative emerging ironmaking technologies for energy-efficiency and carbon dioxide emissions reduction: A technical review. *Renewable and Sustainable Energy Reviews*, 33, pp.645-658.
2. Worldsteel.org. (2019). *Position paper on climate change*. [online] Available at: https://www.worldsteel.org/publications/position-papers/steel-s-contribution-to-a-low-carbon-future.html [Accessed 22 Feb. 2019].
3. Quader, M., Ahmed, S., Ghazilla, R., Ahmed, S. and Dahari, M. (2015). A comprehensive review on energy efficient CO_2 breakthrough technologies for sustainable green iron and steel manufacturing. *Renewable and Sustainable Energy Reviews*, 50, pp.594-614.
4. Junjie, Y. (2018). Progress and Future of Breakthrough Low-carbon Steelmaking Technology (ULCOS) of EU. *International Journal of Mineral Processing and Extractive Metallurgy*, 3(2), p.15.
5. Worldsteel.org. (2019). *ABOUT STEEL*. [online] Available at: https://www.worldsteel.org/about-steel.html [Accessed 22 Feb. 2019].
6. Meijer, K., Guenther, C. and Dry, R. (n.d.). HIsarna Pilot Plant Project. [online] TATA steel, Netherlands, HIsmelt Corp, Kwinana, Australia, pp.1-5. Available at: https://docplayer.net/34533120-Hisarna-pilot-plant-project.html [Accessed 22 Feb. 2019].
7. Van der Stel, J., Meijier, K., Santos, S., Peeters, T. and Broersen, P. (2017). Hisarna, an opportunity for reducing CO_2 emissions from steel industry.
8. Van der Stel, J., Meijer, K., Terrhuis, C., Zaijlstra, C., Keilman, G. and Ouwehand, M. (2013). Update to the developments of Hisarna , An Ulcos alternative ironmaking process.
9. Chen, Z., Qu, Y., Zeilstra, C., van der Stel, J., Sietsma, J. and Yang, Y. (2018). Thermodynamic evaluation for reduction of iron oxide ore particles in a high temperature drop tube furnace. Ironmaking & Steelmaking, pp.1-5.
10. Van der Stel, J., Meijier, K., Santos, S., Peeters, T. and Broersen, P. (2018). Hisarna, Demonstrating low CO_2 ironmaking at pilot scale.
11. Faramawy, S., Zaki, T. and Sakr, A.A.-E. (2016). Natural gas origin, composition, and processing: A review. *Journal of Natural Gas Science and Engineering*, 34, pp.34–54.
12. Jampani, Megha & Pistorius, P. (2014). Increased use of natural gas in blast furnace ironmaking. AISTech - Iron and Steel Technology Conference Proceedings. 1. 593- 601.
13. ATSUSHI, M., UEMURA, H. and SAKAGUCHI, T. (2010). MIDREX Processes. *KOBELCO TECHNOLOGY REVIEW*, [online] 29, pp.50-57. Available at: http://www.kobelco.co.jp/english/ktr/pdf/ktr_29/050-057.pdf [Accessed 22 Jan. 2019].
14. Watson, A. and Valberg, P. (2001). Carbon Black and Soot: Two Different Substances. AIHAJ - American Industrial Hygiene Association, 62(2), pp.218-228.
15. Park, W. and Jung, S. (2014). Effective use of CH_4 gas as a reducing agent in suspension reduction process. *ISIJ International*, 55(1), pp.166-174.
16. Lotfian, S., Ahmed, H., El-Geassy, A.-H.A. and Samuelsson, C. (2016). Alternative Reducing Agents in Metallurgical Processes: Gasification of Shredder Residue Material. *Journal of Sustainable Metallurgy*, 3(2), pp.336–349.
17. Mróz, J. (2001). Evaluation of the reduction of iron oxide from liquid slags using a graphite rotating disk. *Metallurgical and Materials Transactions B*, 32(5), pp.821-830.
18. Sarma, B., Cramb, A. and Fruehan, R. (1996). Reduction of FeO in smelting slags by solid carbon: Experimental results. *Metallurgical and Materials Transactions B*, 27(5), pp.717-730.
19. Min, D., Han, J. and Chung, W. (1999). A study of the reduction rate of FeO in slag by solid carbon. *Metallurgical and Materials Transactions B*, 30(2), pp.215-221.
20. Jouhari, A., Galgali, R., Chattopadhyay, P., Gupta, R. and Ray, H. (2001). Kinetics of iron oxide reduction in molten slag. *Scandinavian Journal of Metallurgy*, 30(1), pp.14-20.
21. TEASDALE, S. and HAYES, P. (2005). Observations of the Reduction of FeO from Slag by Graphite, Coke and Coal Char. *ISIJ International*, 45(5), pp.634-641.
22. TEASDALE, S. and HAYES, P. (2005). Kinetics of Reduction of FeO from Slag by Graphite and Coal Chars. *ISIJ International*, 45(5), pp.642-650.

23. Story, S., Sarma, B., Fruehan, R., Cramb, A. and Belton, G. (1998). Reduction of FeO in smelting slags by solid carbon: Re-examination of the influence of the gas-carbon reaction. *Metallurgical and Materials Transactions B*, 29(4), pp.929-932.
24. Seo, K. and Fruehan, R. (2000). Reduction of FeO in Slag with Coal Char. *ISIJ International*, 40(1), pp.7-15.
25. Fun, F. (1970). Rates and Mechanisms of FeO reduction from slags. *Metallurgical transactions*, 1, pp.2537-2541.
26. JI, F., BARATI, M., COLEY, K. and IRONS, G. (2005). Kinetics of Coal Injection into Iron Oxide Containing Slags. *Canadian Metallurgical Quarterly*, 44(1), pp.85-94.
27. Seo, J. and Kim, S. (1998). Reaction mechanism of FeO reduction by solid and dissolved carbon. *Steel Research*, 69(8), pp.307-311.
28. Bhoi, B., Jouhari, A.K., Ray, H.S. and Misra, V.N. (2006). Smelting reduction reactions by solid carbon using induction furnace: foaming behaviour and kinetics of FeO reduction in CaO–SiO_2–FeO slag. *Ironmaking & Steelmaking*, 33(3), pp.245–252.
29. De Lourdes, M., Gomes, I., Osório, E., Cezar, A. and Vilela, F. (2006). Thermal Analysis Evaluation of the Reactivity of Coal Mixtures for Injection in the Blast Furnace. *Materials Research*, [online] 9(1), pp.91–95. Available at: http://www.scielo.br/pdf/mr/v9n1/28577.pdf.
30. Jalalabadi, T., Li, C., Yi, H. and Lee, D. (2016). A TGA study of CO_2 gasification reaction of various types of coal and biomass. *Journal of Mechanical Science and Technology*, [online] 30(7), pp.3275–3281. Available at: https://link.springer.com/article/10.1007/s12206-016-0636-1 [Accessed 9 Jan. 2020].
31. Wang, G., Zhang, J., Shao, J., Liu, Z., Wang, H., Li, X., Zhang, P., Geng, W. and Zhang, G. (2016). Experimental and modeling studies on CO2 gasification of biomass chars. *Energy*, [online] 114, pp.143–154. Available at: https://www.sciencedirect.com/science/article/pii/S0360544216311057 [Accessed 9 Jan. 2020].
32. Wang, G., Zhang, J., Hou, X., Shao, J. and Geng, W. (2015). Study on CO_2 gasification properties and kinetics of biomass chars and anthracite char. *Bioresource Technology*, [online] 177, pp.66–73. Available at: https://www.sciencedirect.com/science/article/pii/S0960852414016654 [Accessed 9 Jan. 2020].
33. Zhang, X., Song, X., Su, W., Wei, J., Bai, Y. and Yu, G. (2019). In-situ study on gasification reaction characteristics of Ningdong coal chars with CO2. *Journal of Fuel Chemistry and Technology*, 47(4), pp.385–392.
34. NETZSCH Analiza i testy. (2019). *STA 449 F3 Jupiter®*. [online] Available at: https://www.netzsch-thermal-analysis.com/pl/produkty-rozwiazania/jednoczesna-analiza-termiczna/sta-449-f3-jupiter/ [Accessed 12 Dec. 2019].
35. Dakič, D., van der Honing, G. and Valk, M. (1989). Fragmentation and swelling of various coals during devolatilization in a fluidized bed. *Fuel*, 68(7), pp.911–916.
36. Seo, D.K., Lee, S.K., Kang, M.W., Hwang, J. and Yu, T.-U. (2010). Gasification reactivity of biomass chars with CO_2. *Biomass and Bioenergy*, 34(12), pp.1946–1953.
37. Li, S. and Cheng, Y. (1995). Catalytic gasification of gas-coal char in CO_2. *Fuel*, 74(3), pp.456–458.
38. Sircar, I., Sane, A., Wang, W. and Gore, J. P. (2014). Experimental and modeling study of pinewood char gasification with CO2. *Fuel*, 119, pp.38–46.
39. Lotfian, S., Ahmed, H., El-Geassy, A.-H.A. and Samuelsson, C. (2016b). Alternative Reducing Agents in Metallurgical Processes: Gasification of Shredder Residue Material. *Journal of Sustainable Metallurgy*, 3(2), pp.336–349.
40. Zhang, Y., Hara, S., Kajitani, S. and Ashizawa, M. (2010). Modeling of catalytic gasification kinetics of coal char and carbon. *Fuel*, 89(1), pp.152–157.
41. Thommes, M., Kaneko, K., Neimark, A.V., Olivier, J.P., Rodriguez-Reinoso, F., Rouquerol, J. and Sing, K.S.W. (2015). Physisorption of gases, with special reference to the evaluation of surface area and pore size distribution (IUPAC Technical Report). *Pure and Applied Chemistry*, [online] 87(9–10), pp.1051–1069.
42. Gargiulo, V., Gomis-Berenguer, A., Giudicianni, P., Ania, C.O., Ragucci, R. and Alfè, M. (2018). Assessing the Potential of Biochars Prepared by Steam-Assisted Slow Pyrolysis for CO2 Adsorption and Separation. *Energy & Fuels*, 32(10), pp.10218–10227.
43. Lu, H., Ip, E., Scott, J., Foster, P., Vickers, M. and Baxter, L.L. (2010). Effects of particle shape and size on devolatilization of biomass particle. *Fuel*, 89(5), pp.1156–1168.
44. Lahijani, P., Zainal, Z.A., Mohamed, A.R. and Mohammadi, M. (2013). CO_2 gasification reactivity of biomass char: Catalytic influence of alkali, alkaline earth and transition metal salts. *Bioresource Technology*, 144, pp.288–295.
45. Bouraoui, Z., Jeguirim, M., Guizani, C., Limousy, L., Dupont, C. and Gadiou, R. (2015). Thermogravimetric study on the influence of structural, textural and chemical properties of biomass chars on CO_2 gasification reactivity. *Energy*, 88, pp.703–710.
46. Ke-Chang Xie and Springer-Verlag Gmbh (2016). *Structure and Reactivity of Coal A Survey of Selected Chinese Coals*. Berlin Springer Berlin Springer.
47. Zhou, L., Zhang, G., Schurz, M., Steffen, K. and Meyer, B. (2016). Kinetic study on CO_2 gasification of brown coal and biomass chars: reaction order. *Fuel*, [online] 173, pp.311–319. Available at: https://www.sciencedirect.com/science/article/pii/S0016236116000569 [Accessed 9 Jan. 2020].

48. De Micco, G., Nasjleti, A. and Bohé, A.E. (2012). Kinetics of the gasification of a Rio Turbio coal under different pyrolysis temperatures. *Fuel*, 95, pp.537–543.
49. Kim, Y.T., Seo, D.K. and Hwang, J. (2011). Study of the Effect of Coal Type and Particle Size on Char–CO_2 Gasification via Gas Analysis. *Energy & Fuels*, 25(11), pp.5044–5054.
50. Zhang, X., Yan, Q., Leng, W., Li, J., Zhang, J., Cai, Z. and Hassan, E. (2017). Carbon Nanostructure of Kraft Lignin Thermally Treated at 500 to 1000 °C. *Materials*, [online] 10(8), p.975. Available at: https://pdfs.semanticscholar.org/1a5b/d660bea08349801a9abd86f1b54924308cdb.pdf [Accessed 14 Jan. 2020].
51. Ramamurti, R., Shanov, V., Singh, R.N., Mamedov, S. and Boolchand, P. (2006). Raman spectroscopy study of the influence of processing conditions on the structure of polycrystalline diamond films. *Journal of Vacuum Science & Technology A: Vacuum, Surfaces, and Films*, [online] 24(2), pp.179–189. Available at: https://avs.scitation.org/doi/10.1116/1.2150228 [Accessed 15 Jan. 2020].
52. Sonibare, O.O., Haeger, T. and Foley, S.F. (2010). Structural characterization of Nigerian coals by X-ray diffraction, Raman and FTIR spectroscopy. *Energy*, [online] 35(12), pp.5347–5353. Available at: https://www.sciencedirect.com/science/article/pii/S0360544210004007 [Accessed 14 Jan. 2020].
53. Jawhari, T., Roid, A. and Casado, J. (1995). Raman spectroscopic characterization of some commercially available carbon black materials. *Carbon*, [online] 33(11), pp.1561–1565. Available at: https://www.sciencedirect.com/science/article/pii/000862239500117V [Accessed 14 Jan. 2020].
54. Zhao, Y., Zhang, Y., Zhang, H., Wang, Q. and Guo, Y. (2015). Structural characterization of carbonized briquette obtained from anthracite powder. *Journal of Analytical and Applied Pyrolysis*, [online] 112, pp.290–297. Available at: https://www.sciencedirect.com/science/article/pii/S0165237015000212 [Accessed 14 Jan. 2020].
55. Kramb, J., Gómez-Barea, A., DeMartini, N., Romar, H., Doddapaneni, T.R.K.C. and Konttinen, J. (2017). The effects of calcium and potassium on CO_2 gasification of birch wood in a fluidized bed. *Fuel*, 196, pp.398–407.
56. McKee, D.W., Spiro, C.L., Kosky, P.G. and Lamby, E.J. (1983). Catalysis of coal char gasification by alkali metal salts. *Fuel*, 62(2), pp.217–220.
57. McKee, D.W. (1983). Mechanisms of the alkali metal catalysed gasification of carbon. *Fuel*, 62(2), pp.170–175.

Figure

Click here to access/download;Figure;figure1.tif

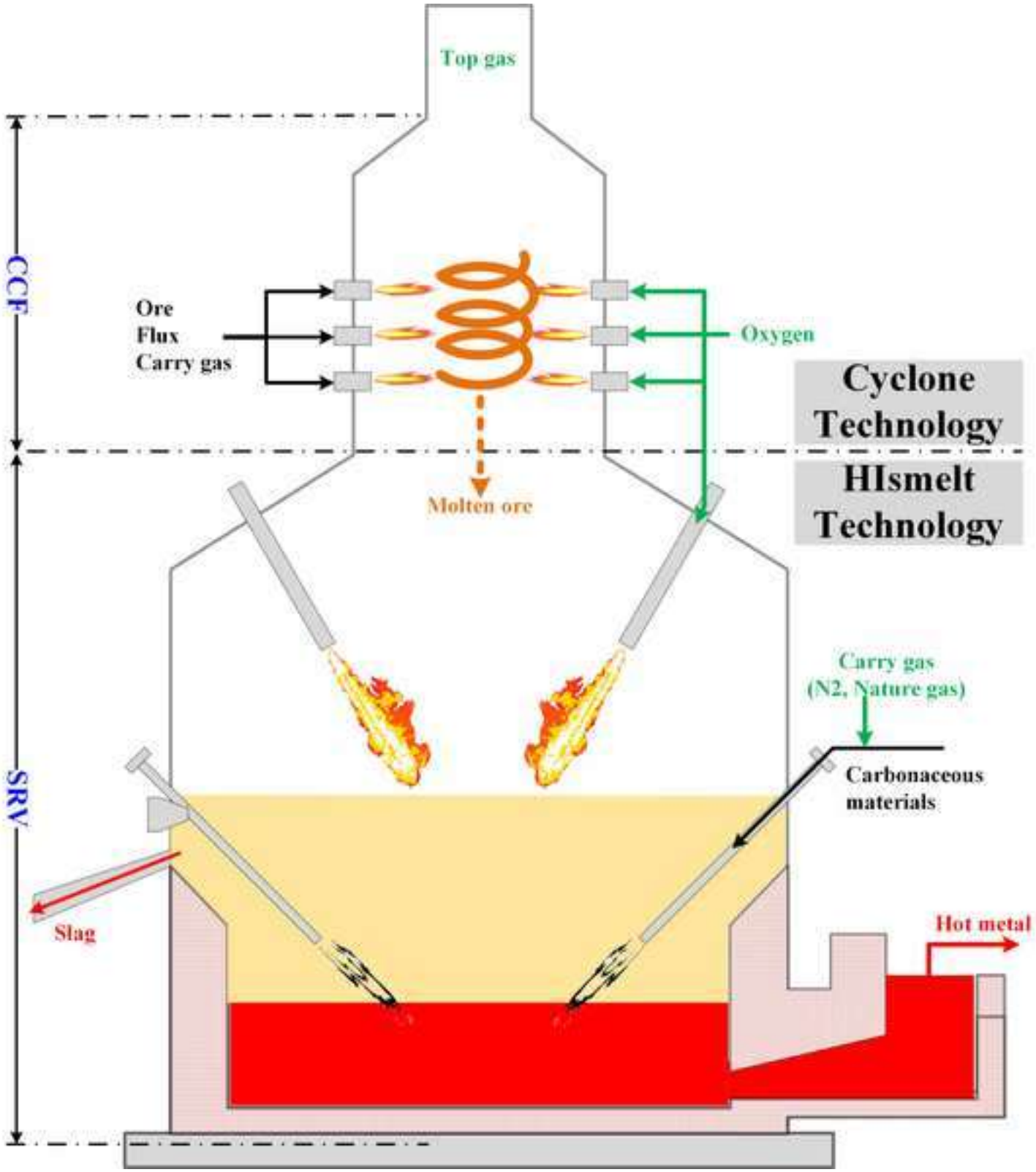

Figure

Click here to access/download;Figure;figure 2.tif

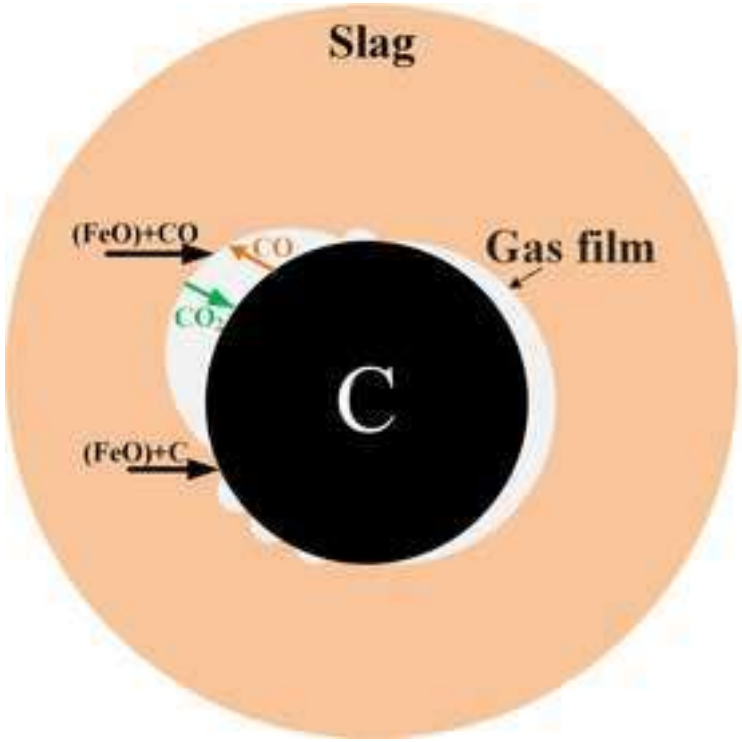

$$(FeO) + C\,(s) = [Fe] + CO\,(g) \qquad (2)$$

$$(FeO) + CO\,(g) = [Fe] + CO_2\,(g) \qquad (3)$$

$$CO_2\,(g) + C\,(s) = 2\,CO\,(g) \qquad (4)$$

Figure

Click here to access/download;Figure;figure3.tif

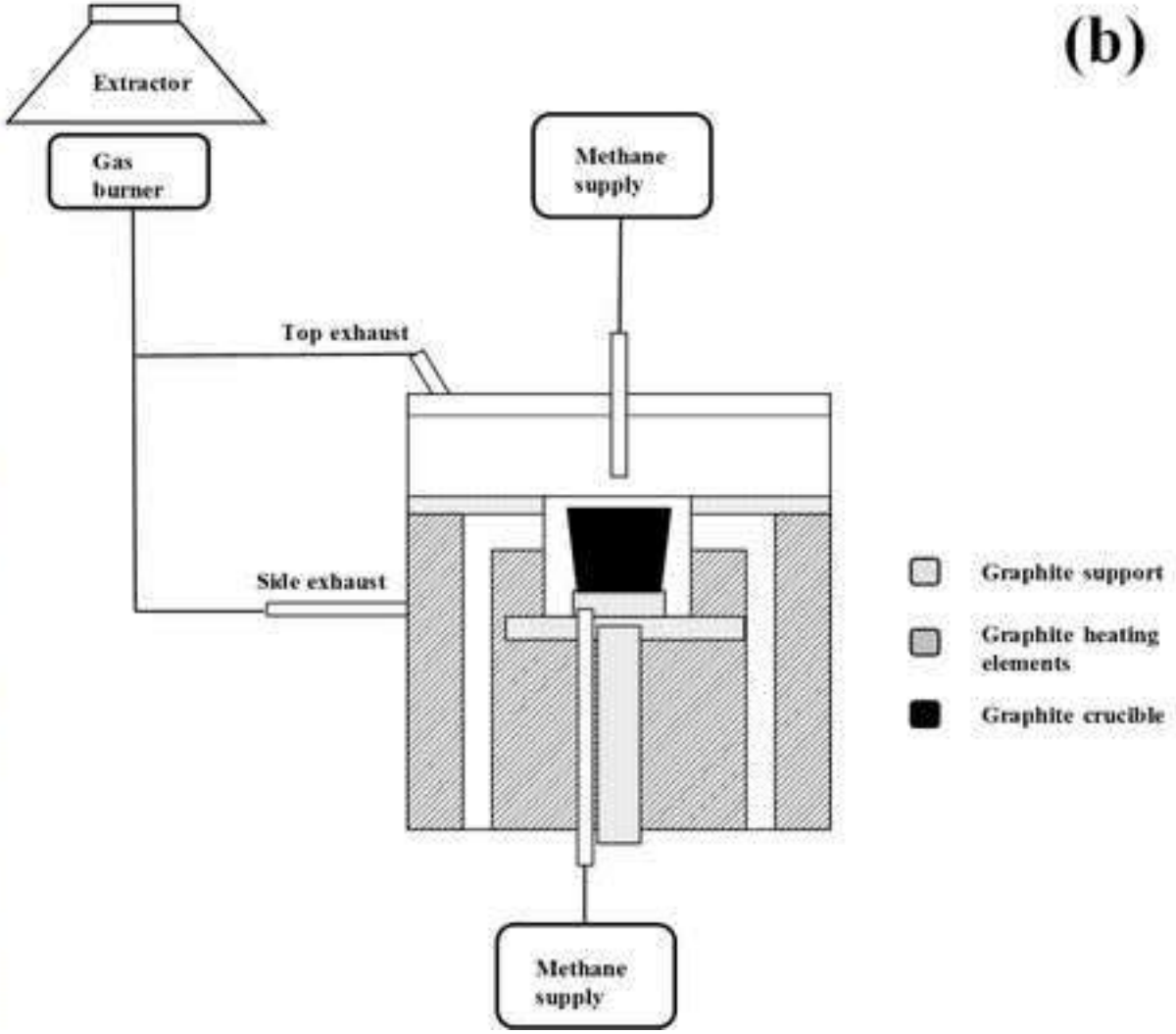

Figure

Click here to access/download;Figure;figure4.tif

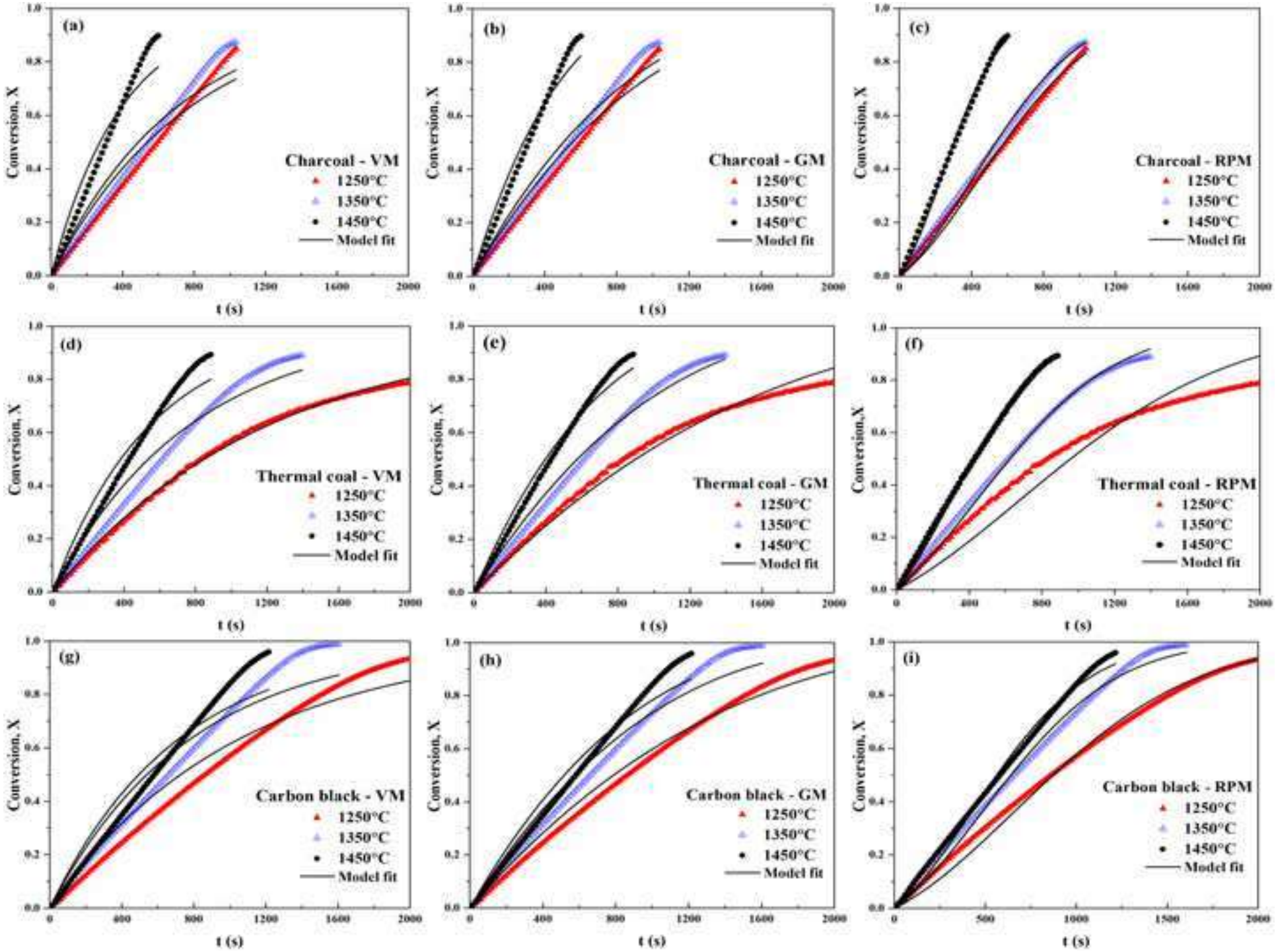

Figure

Click here to access/download;Figure;figure5.tif

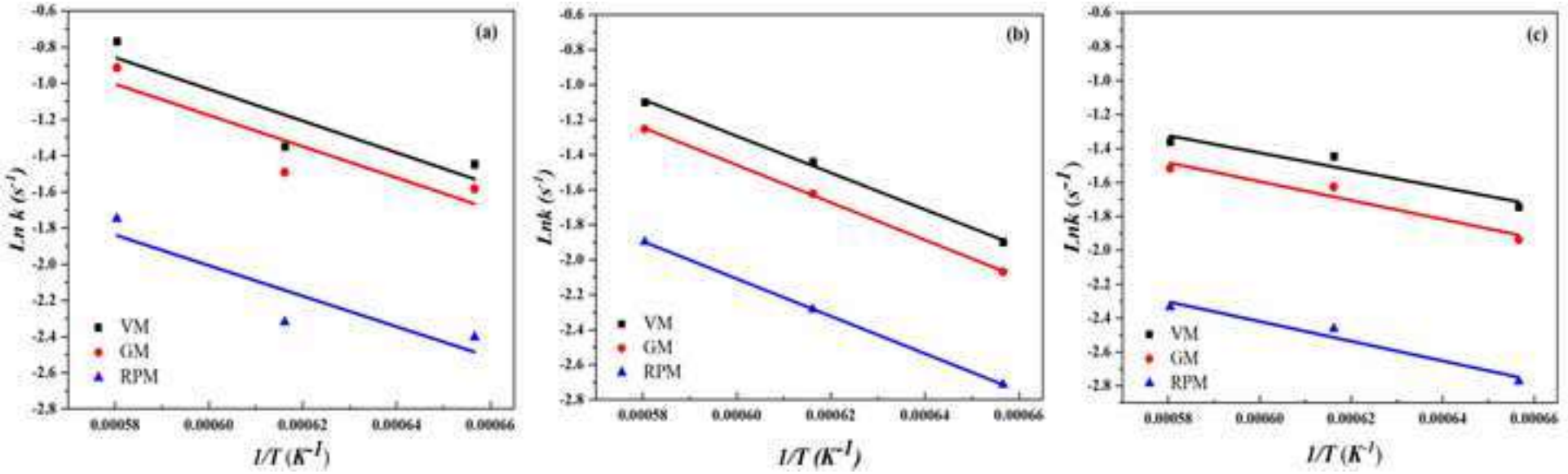

Figure

Click here to access/download;Figure;Figure 6.tif

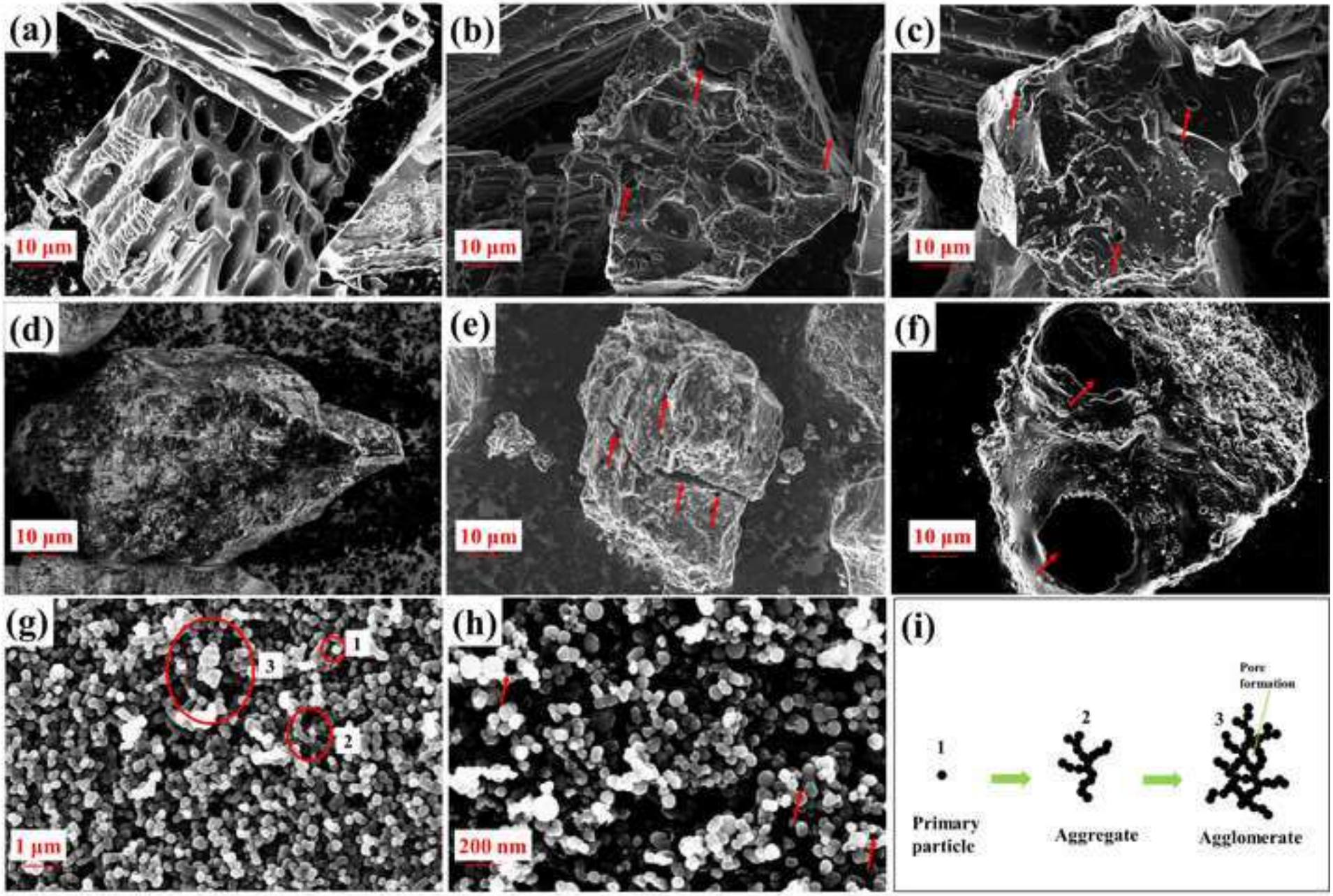

Figure

Click here to access/download;Figure;Figure7.tif

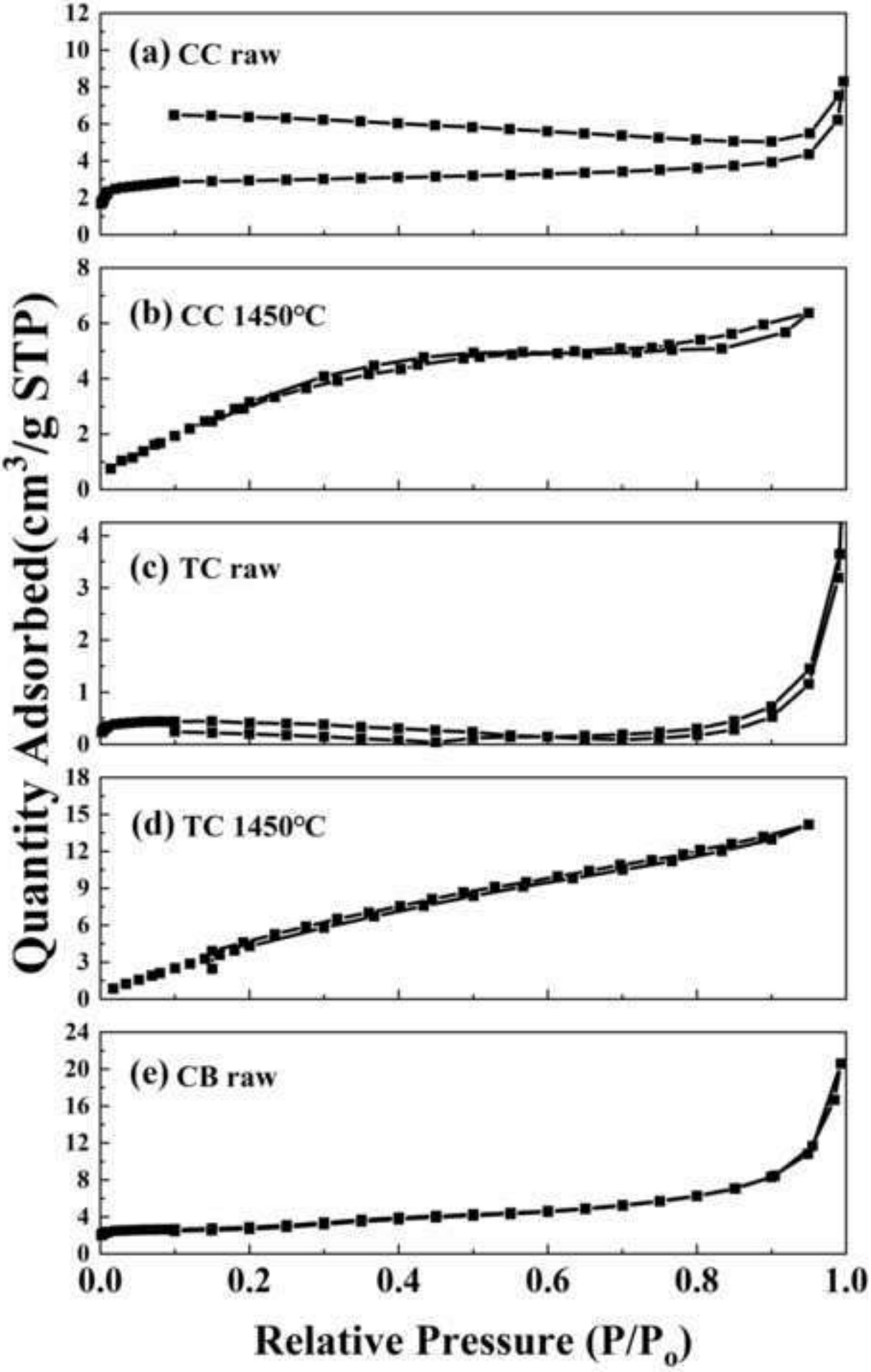

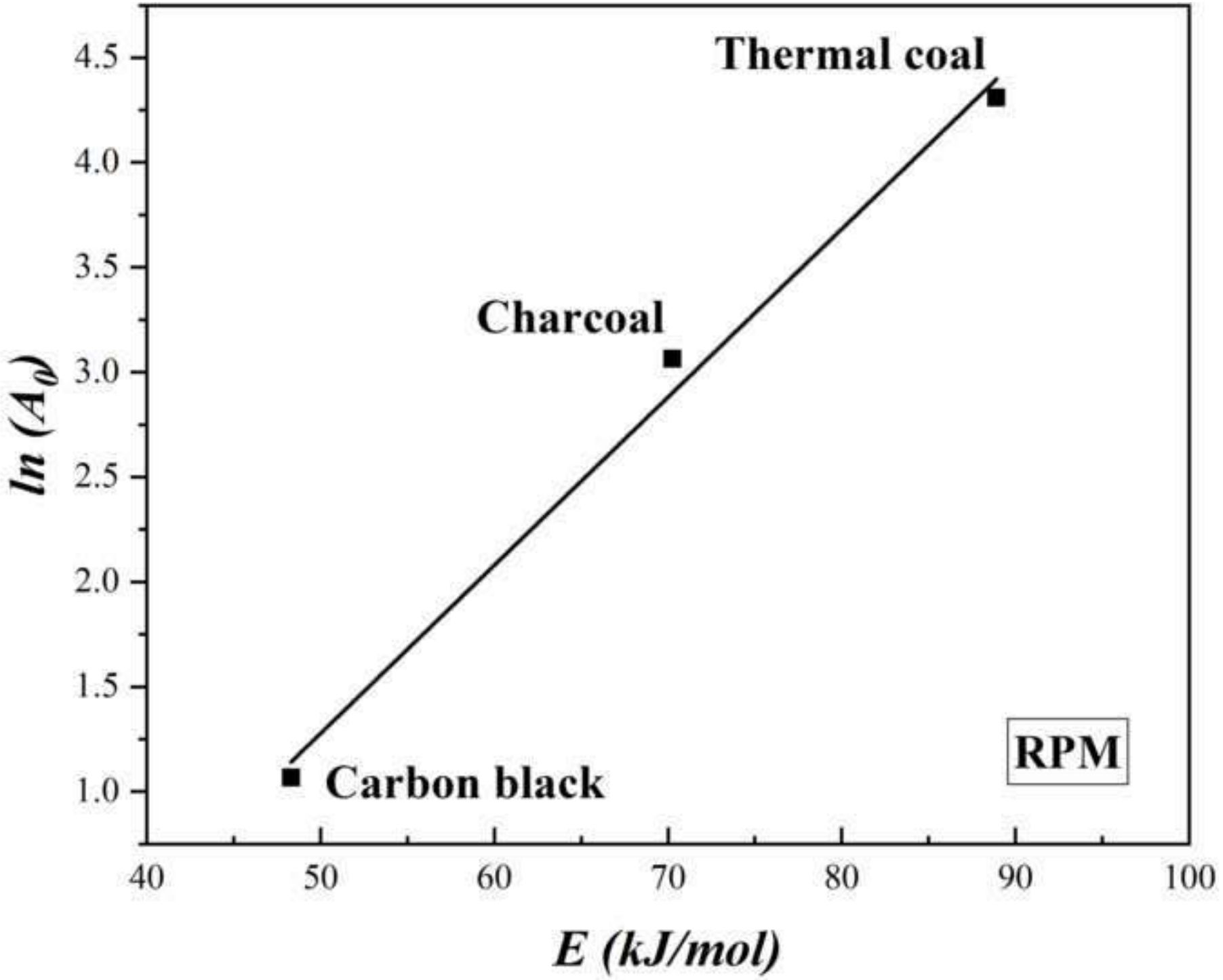

Figure

Click here to access/download;Figure;figure 9.tif

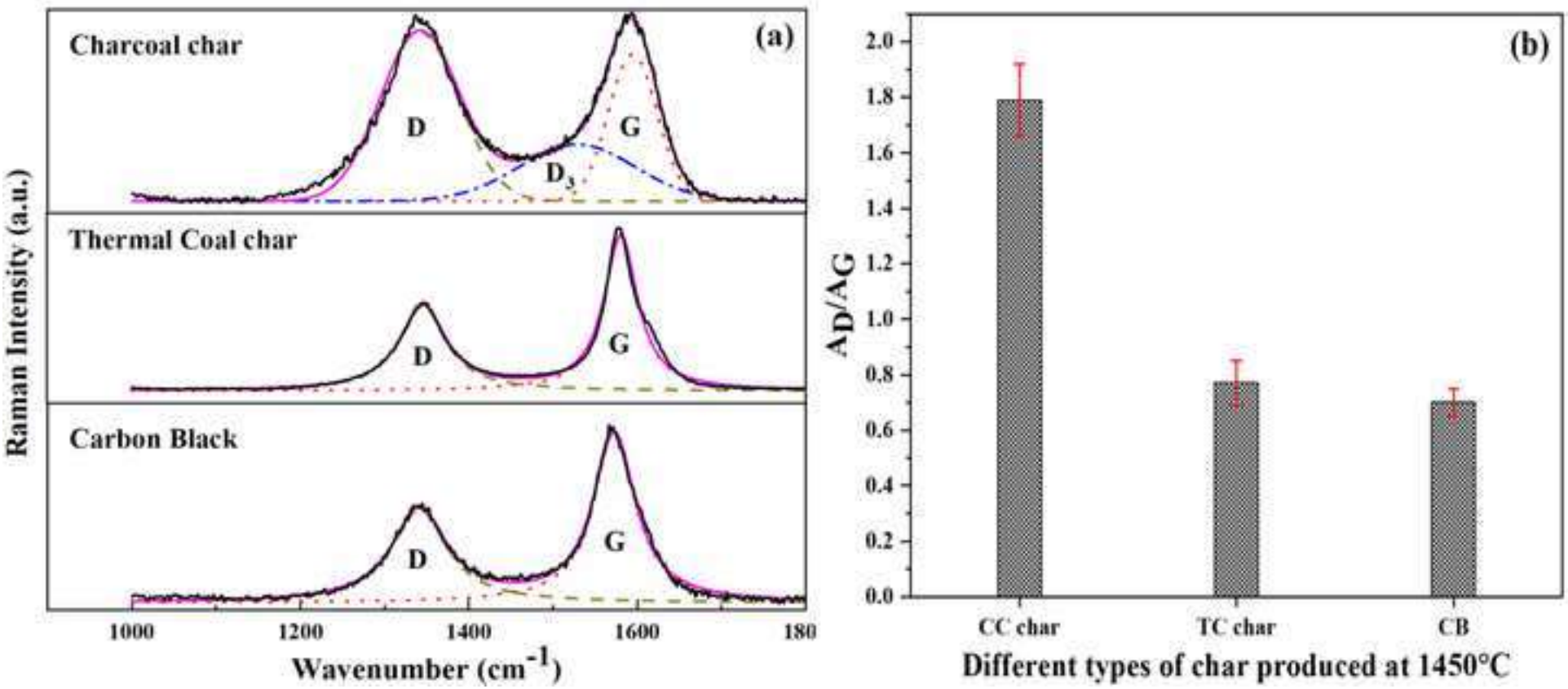

*Declaration of Interest Statement

Declaration of interests

☒ The authors declare that they have no known competing financial interests or personal relationships that could have appeared to influence the work reported in this paper.

☐The authors declare the following financial interests/personal relationships which may be considered as potential competing interests:

Credit author statement

Theint Theint Htet: Conceptualization, Formal analysis, Investigation, Methodology, Writing-original draft.

Zhiming Yan*: Supervision, Software, Writing-review & editing.

Stephen Spooner: Supervision.

Volkan Degirmenci: Data curation for BET section.

Koen Meijer: Resources, Supervision.

Zushu Li: Funding acquisition, Supervision, Writing-review & editing.